IEEE JOURNAL OF OCEANIC ENGINEERING, VOL. 27, NO. 3, JULY 2002, 717-725.

A Three Component Bistatic Coherent Doppler Velocity Profiler: Error Sensitivity and System Accuracy

L. Zedel[1], A.E. Hay[2]

[1] Memorial University of Newfoundland, St. John's, NF
[2] Dalhousie University, Halifax, NS

Abstract - We report on a 1.7 MHz coherent Doppler sonar system designed for near-shore environments that provides three component velocity profiles over an O(0.5 m) depth range. The use of a bistatic geometry allows three independent components of velocity to be measured simultaneously in time and coincident in space. The system was calibrated in a tow-tank facility for horizontal velocities up to 2 m/s. For multiple pulse-pair ensemble-averaged velocity estimates generated at a rate of 30 profiles/second in 0.7 cm depth bins, the standard deviation in measured vertical velocity is about 1 % of the total flow speed. For the horizontal components (based on bistatic measurements) the standard deviation of velocity estimates is about 5%. Absolute accuracies are also about 5% of the speed but a portion of this bias is caused by flow disturbance around the instrument package: this disturbance is modeled using potential flow past a cylinder.

I. Introduction

Velocity measurements over length scales of O(0.5 m) with centimeter resolution are required to investigate sediment transport in the wave-current bottom boundary layer of the near-shore zone. The small scales of measurement and the short ranges involved are such that point sensors mounted near the bed can cause flow disturbance and degrade data quality. In this environment, acoustic sampling can provide an attractive alternative to point sensor measurements. Suspended sediment concentration can be determined from acoustic backscatter intensity, (see [1]), and velocity can be determined using Doppler sonar (see [2]). These remote profiling techniques are non-invasive, robust, and can be deployed in both field and laboratory applications.

Doppler sonar systems measure velocity by recording frequency shifts in sound scattered by objects in the water such as sand, zooplankton and even temperature microstructure. For the case that the scatterers are moving as passive tracers of water motion, the Doppler sonar measures water velocity. It is possible to directly analyze the frequency content of backscattered sound to establish the "Doppler" shift; this technique is called the incoherent or narrow-band method. The accuracy of the incoherent approach is limited by the bandwidth of the scattered sound (see discussions by [3]). Much greater accuracy can be achieved by using pulse-to-pulse coherent sonar systems (see [4] and [2]). These systems transmit pairs of acoustic pulses or codes and the speed of the scatterers is determined by measuring the change in phase of sound scattered by successive pulses (see [5]). A complication arises with coherent sonars because the observed phase change has a $\pm\pi$ radian ambiguity. This phase ambiguity translates into an ambiguity velocity or a maximum unambiguous velocity that can be resolved by a system. Observations in excess of the ambiguity velocity are possible but only while the transitions across the ambiguity velocity can be tracked.

The component of velocity measured by a Doppler sonar system is determined by the system geometry. Most systems operate in a monostatic backscatter geometry for which velocity measurements are made along a narrow acoustic beam. Profiles over depth are achieved by range gating the backscattered sound. In order to measure other velocity components, multiple acoustic beams can be used or a bistatic geometry must be employed [6]. A drawback of most bistatic beam geometries is that the sample volume is defined by the intersection of the two beams. As a result, they cannot use the range gating technique to achieve measurement profiles.

In this paper, we describe a bistatic sonar system assembled from the modular coherent sonar units described in [2]. Three component velocity profiles are achieved by using beam patterns with a large intersecting volume and range gating of the scattered sound. We report on calibration tests of this system made in a tow-tank facility. The vertical velocity component can be measured with an uncertainty of about 1% of the total flow speed (dominated by horizontal components). The accuracy of the horizontal velocity measurements is limited to about 5% by instrument effects. Bias in the horizontal measurements is caused by flow disturbance around the instrument package.

II. System Configuration

Bistatic geometries have been used with intersecting narrow beams to produce a single point measurement in the intersection zone ([7]). Good localization of the sample volume is achieved but the region that can be sampled by the system is limited. We overcome this problem by employing one beam with a narrow, radially symmetric beam pattern and a second beam with a fan shaped pattern as shown in Fig. 1. The symmetrical beam (Fig. 1b) is oriented vertically with the fan beam intersecting at an oblique angle as indicated in Fig. 2. The vertical sonar operates as a monostatic coherent Doppler system and provides a direct measurement of vertical velocities. The fan beam of the passive sonar also receives backscatter from the active sonar system and this signal is used to make bistatic velocity measurements.

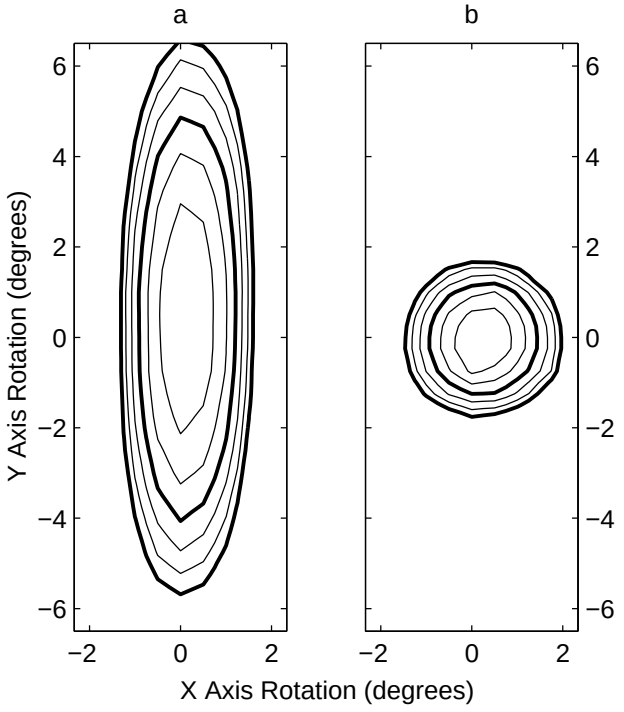

Figure 1: Acoustic beam patterns used for bistatic profiling, a) fan beam, and b) symmetrical beam. For both figures, the axes indicate the angle in degrees from an arbitrary direction close to the beam axis. Relative power is indicated by contours in increments of 1 dB relative to peak power, -3 and -6 dB contours are drawn in bold.

In monostatic Doppler, frequency shifts result when the distance between the transceiver and the scatterer changes with time. Motion along spherical surfaces (at a constant distance from the transmitter) result in no Doppler shift; only the component of motion radial to the transceiver is measured. For the bistatic system, the distance being measured is from the transmitter to the scatterer and then to the receiver. This geometry defines an ellipsoidal surface and the bistatic Doppler measures motion normal to that ellipsoidal surface. The bistatic scattering geometry is indicated in Fig. 2a.

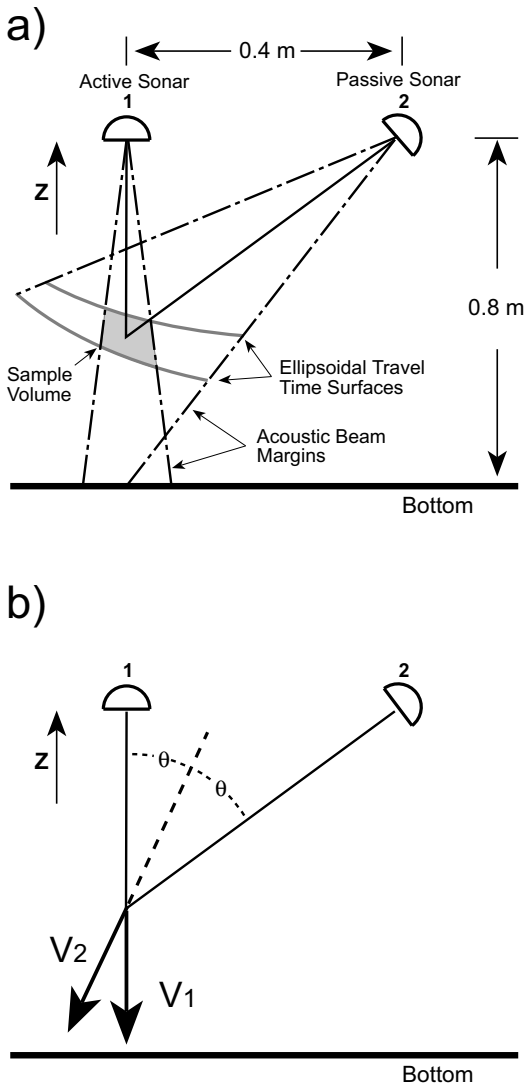

Figure 2: a) Sectional view of intersecting beam patterns (as taken along the line A-A' in Figure 3b). Beam edges are indicated by dash-dot lines. Range gating of the backscattered data defines ellipsoidal travel time surfaces in space. The sample volume (shaded region) is defined by the intersection of the two beam patterns and range gated travel time surfaces. The scattering geometry for a representative point in the sample volume is indicated by solid lines. b) Geometry of measured velocity components. The resolved velocity component V_2 is at an angle θ relative to the vertical axis and the directly measured vertical velocity V_1.

The intersecting beam patterns serve to define the sample volume in two dimensions. The third dimension is constrained by range gating the backscattered

signal. The range gates define ellipsoidal travel time surfaces governed by the same geometrical argument that regulates the bistatic velocity measurement. The sample volume is indicated in Fig. 2a, and the measured components of velocity are indicated in Fig. 2b. The active (vertical) sonar transmits 9.3 μs pulses, sample range gates in both the active and passive systems are 9.3 μs corresponding to depth cells of about 0.7 cm.

The sample geometry indicated in Fig. 2a allows the measurement of velocity in two dimensions. Three component profiles are acquired by making an additional independent velocity measurement with a second passive transducer using the same geometry as indicated in Fig. 2, but in a different vertical plane (see Fig. 3a). Vectors labeled V_2 and V_3 in Fig. 3b indicate the horizontal projection of the observed velocities: we have selected a geometry with the angle ϕ different from 90° because of mechanical constraints encountered in mounting the transducer systems (see Fig. 3b). The plane of view used in Fig. 2 is indicated in Fig. 3 by the line A-A'. Fig. 3b defines the right handed coordinate system used with the z-axis oriented up out of the diagram, velocity vectors U, V and W correspond to the X, Y, and Z coordinates.

The beam patterns are not simple conical domains as implied by Fig. 2, but lobed structures as shown in Fig. 1. Rather than a well defined linear sample domain, the measurement profile describes a curve that wanders over several centimeters in the horizontal. These slight shifts in sample location affect the values of θ and ϕ which determine the velocity component being measured. The sensitivity of resolved velocity is indicated in Figure 4 by the velocity error that results from a given error in horizontal position (at a range of 60 cm). Using Figure 4 as a guide, the sample volume must be identified to within 1 cm to provide velocity accuracies of 1%.

In order to establish the exact sample geometry for each range gate, the measured beam patterns for the three transducers must be used to reconstruct the beam pattern intersection in three dimensions. The effective sample points are then found by determining the intensity weighted centroid for any range gate. Fig. 5 depicts a 2-dimensional projection of the sample domain with the dashed (black and white) line indicating the resulting sample profile. Three component velocities can only be recovered from that region where significant beam overlap occurs. For the geometry indicated in Fig. 5, good profile data can be recovered from the region between 50 and 85 cm below the transducers. Greater regions of overlap could be realized by re-adjusting the system for an intersection point at greater depth or by decreasing the spacing between the transducers. Both of these

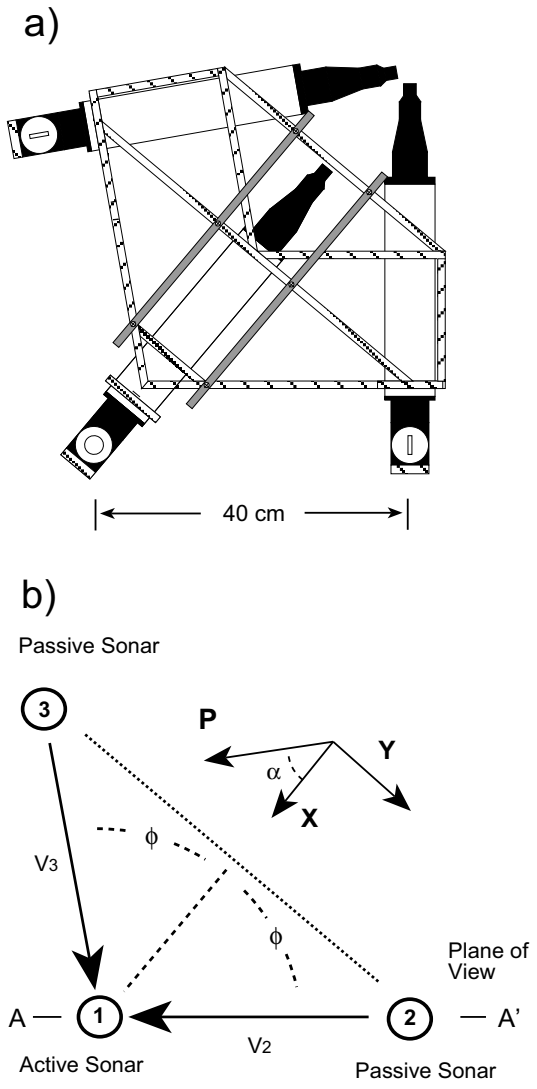

Figure 3: a) Schematic diagram, and b) plan layout of bistatic transducer array defining the sample locations and coordinate system (the z-axis is directed upwards out of the page). The resolved components of velocity are indicated by arrows labeled V_2 and V_3, the plane of view shown in Fig. 2 is indicated by the line A-A'. The vector **P** identifies the horizontal component of velocity observed when the instrument assembly was rotated by an angle α with respect to the tow-tank axis.

changes would also affect system accuracy through changes in the system geometry.

Once the exact profile location has been determined, the angles θ and ϕ can be found for each depth bin and each transducer pair. The vertical component of velocity is resolved directly by the vertical sonar system (transducer 1). The two orthogonal components in the horizontal plane (U, V) require a transformation from the measured coordinate system. This transformation involves values of θ and ϕ for each depth bin and for the two passive trans-

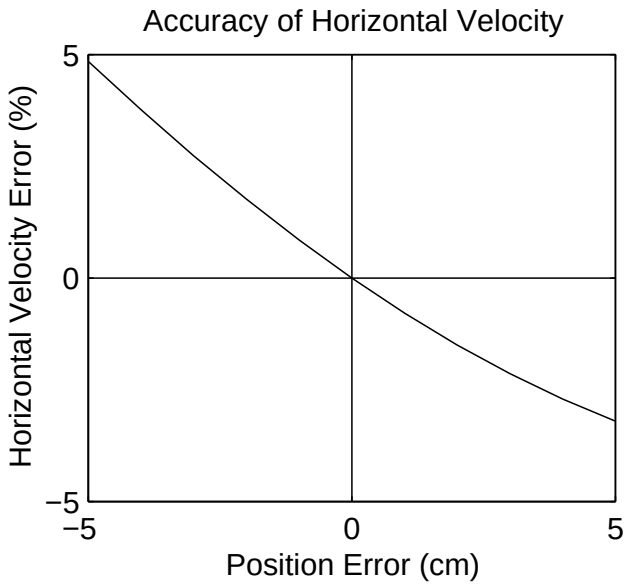

Figure 4: Relationship between errors in horizontal position of the sample volume at a range of 60 cm and the associated error in resolved horizontal velocity.

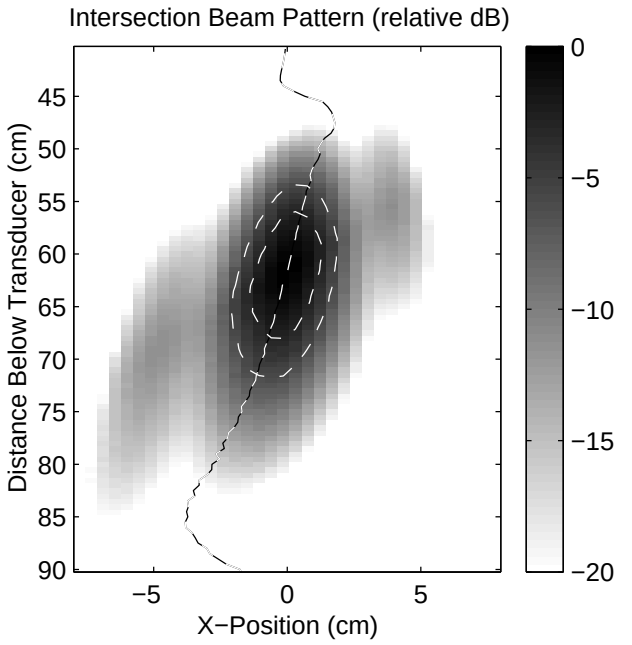

Figure 5: Two dimensional projection of the intersecting beam patterns for the bistatic geometry described by Fig. 2. The grey scale represents the relative backscatter contribution in dB, the -3 and -6 dB points are indicated by the dashed white lines. The backscatter centroid (which determines the sample locations) is shown by the black and white dashed line.

ducers. While we employ the complete transformation in the data reduction, a simplification that retains the dominant characteristics can be realized if θ and ϕ are assumed identical for the two passive transducers. In this case,

$$U = \frac{V_2 + V_3 - 2V_1 \cos\theta}{2 \sin\theta \cos\phi} \tag{1}$$

and

$$V = \frac{V_3 - V_2}{2 \sin\theta \sin\phi}. \tag{2}$$

where V_1, V_2, and V_3 refer to the velocities measured by transducers 1, 2, and 3 respectively. It is important to note that (2) does not contain any terms in V_1; in the fully resolved equations the coefficient scaling the V_1 component is small. The V_1 term is absent in (2) because the vertical velocity component is canceled in forming $V_3 - V_2$.

III. Velocity Variance

The accuracy constraints for monostatic coherent Doppler sonar systems are well characterized [2]. In the bistatic case, additional errors are introduced through uncertainties in the angles ϕ and θ and the need to combine three velocity measurements. We use a tow-tank facility measuring 65 m × 5 m with a 1.8 m depth to test the system accuracy. The sonar array is mounted on a carriage which can travel the length of the tank with a speed controlled to an accuracy of ± 5 mm s^{-1} as determined by a mechanically activated speed indicator. Calibrations were undertaken with the sonar rotated through 10 degree increments about the z-axis (the resulting current velocity for positive tow directions and rotation angle α is identified by the vector $\mathbf{P}$ in Fig. 3b). At each rotation, data at a variety of carriage speeds were collected to a maximum of 2 m s^{-1}. In all cases, an adequate concentration of scatterers was ensured by adding quantities of agricultural lime to the tow-tank (typically at a rate of 10 kg/day of testing).

The Doppler system was configured to transmit 9.3 μs pulses at a rate of 500 s^{-1} averaging each 10 transmissions into a profile. Including computational overhead, complete averaged profiles are created at a rate of 30 s^{-1}. In this configuration, the limiting accuracy of the monostatic system is about ±0.1 cm s^{-1} [2]. We would expect similar performance for the individual velocity components of the bistatic systems as these are essentially the same measurement (but with a different geometry). Fig. 6 compares the observed standard deviations in data from the 3 sonar beams (beam 1 is the vertical, monostatic system) for a variety of carriage tow speeds. The data shown in Fig. 6 are based on observations at a range of 60-65 cm with the instrument rotated so that tow speeds are in the ±Y direction (corresponding to $\alpha = -90°$ in Fig. 3b),

each data point is based on at least 250 observations, data are plotted for both positive and negative tow directions. The velocity standard deviations are comparable between the three components all increasing as tow speeds increase. The anomalous high variance values that are seen in beams 2 and 3 at low carriage speeds are a result of low signal levels; at higher tow speeds, stirring of the tank enhances suspension of the powdered lime. Notice that the Y-intercept of all the curves is close to 0.1 cm s^{-1}; the expected limiting accuracy of the system.

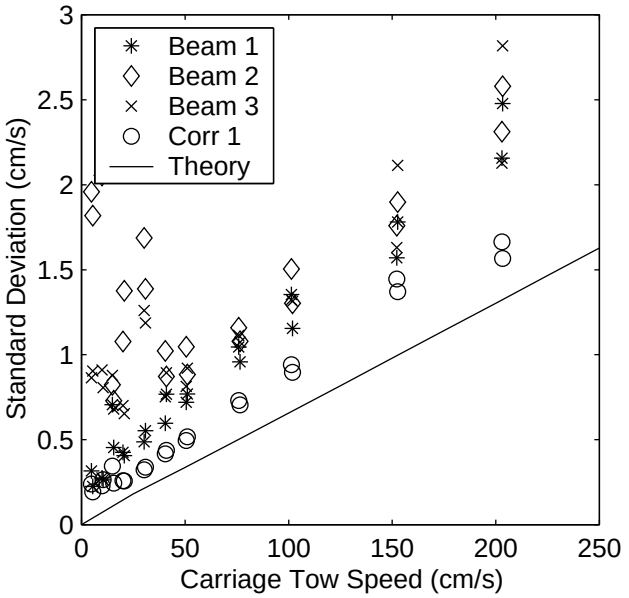

Figure 6: Standard deviations of the measured component velocities taken from between 60 to 65 cm below the transducers. Beams 1, 2, and 3 refer to the data collected by sonar systems 1, 2, and 3. Beam 1 is the monostatic, vertically oriented system. True velocities are in the Y direction so that both of the bistatic systems see the same magnitude velocity component. Data are based on at least 250 independent observations. Large variance at low speeds in beam 2 and 3 is caused by low scatterer concentrations. Standard deviations anticipated based on signal correlation coefficient (for beam 1) are indicated by Corr1, the straight line indicates the theoretically predicted values using (5) and (6).

Standard deviations of the resolved velocity components are increased because of the need to combine measurements and the use of geometrical scalings. Fig. 7 shows how standard deviations at a depth of between 60 and 65 cm below the transducers vary with increasing tow speed. Data shown in Fig. 7 are the same as were used in Fig. 6. The vertical component is based only on the monostatic beam data so that it repeats the data shown in Fig. 6. Both of the horizontal components show larger errors than the vertical component with the deviations in U being larger than those in V (even at low speeds). The results are the same for both positive and negative directions of motion. Uncertainties here are no more than 5% of the tow speed.

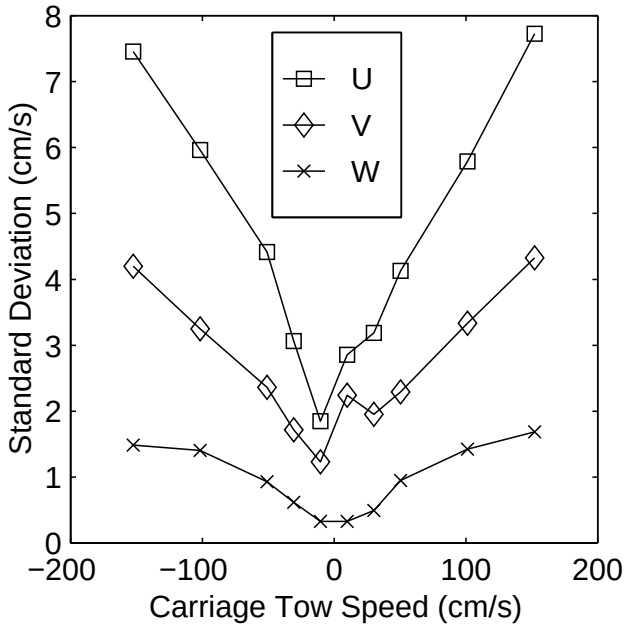

Figure 7: Standard deviation of resolved velocity for the same data shown in Fig. 6. For these data the U and W components of velocity are zero.

The larger uncertainties in the U component compared to the V component are a consistent result irrespective of system orientation. The cause of this difference stems from the asymmetry in (1) and (2). It can be assumed that all of the component velocity estimates (V_1, V_2, and V_3) have comparable uncertainties consistent with data shown in Fig. 6. When these uncertainties are combined through (1) and (2) the resulting uncertainty in resolved velocities can be found as:

$$\sigma_u = \sigma \frac{(2 + 4\,cos^2\,\theta)^{1/2}}{2\,sin\,\theta\,cos\,\phi} \tag{3}$$

for the U component and

$$\sigma_v = \sigma \frac{2^{1/2}}{2\,sin\,\theta\,sin\,\phi} x, \tag{4}$$

for the V component, where σ is the uncertainty in the individual beam velocity estimates. For values of $\theta \simeq 30°$, $\sigma_u/\sigma_v \simeq 1.4$. The minimum of σ_u/σ_v for the data shown in Fig. 7 is 1.3 and the mean is 1.6, consistent with (3), and (4).

IV. Tank Turbulence

In using the tow-tank as a calibration facility, we are assuming that there is no turbulence present in the tank. Residual turbulence and surface waves

caused by the successive passes of the instrumentation through the tow-tank will introduce variance into the velocity estimates. The tow-tank data can only be used to characterize system performance if the actual velocity fluctuations in the tow-tank are small compared to the accuracy of the measurements. In fact, power spectra of the vertical velocity measurements do show a -5/3 slope indicating that turbulence is present in these data. This spectral character is not seen in the horizontal velocity estimates because of the reduced accuracy in these derived components. We can make some estimate of the relative contribution of this contamination by comparing the present results with theoretical predictions given by [2].

Data quality from individual acoustic returns is tracked by monitoring the correlation coefficient between successive acoustic pulses. The correlation coefficients for the beam data can be translated into an associated velocity standard deviations by rearranging equation 8 given by [2] to:

$$\sigma_v = \frac{-C\sqrt{ln\, R^2}}{\sqrt{2}\pi\tau f}/\sqrt{n-1}, \qquad (5)$$

where C = sound speed, R is the correlation coefficient, τ is the time between acoustic pulses, f is the acoustic frequency, and n is the number of transmissions averaged. This estimate includes only variance that is caused by velocity fluctuations occurring on length scales smaller than the sample volume (about 1 cm in the present case) and instrumentation noise. Importantly, it excludes any variance that is caused by large scale motions in the tank such as might be associated with waves or flows induced by successive passages of the instrumentation. As such, it indicates the variance that would be realized if there were no physical sources of variance in the sample data. Uncertainties as estimated using (5) with beam 1 correlation coefficients are indicated by circles in Fig. 6. The observations suggest that about 20% of the standard deviations recorded are introduced by residual motions in the tank.

In the absence of turbulent velocities, the dominant source of variance in the velocity signal is the passage of scatterers through the acoustic beam. Scatterers that are present in the beam during the passage of both acoustic pulses contribute to a coherent evolution of backscatter phase from which velocity can be estimated. Scatterers that enter or depart beam in the time between acoustic pulses contribute incoherent backscatter with a random phase which degrades the velocity estimate. Theoretical estimates of the standard deviation associated with this process can be determined by considering the beam pattern, transmit pulse and tow speed using equation 10 given by [2]:

$$R^2 = \frac{\int D^2(\vec{r}) e^{2\,i\,\vec{k}\cdot\vec{r}}\, D^2(\vec{r}+\vec{v}_t\tau) e^{-2\,i\,\vec{k}\cdot(\vec{r}+\vec{v}_t\tau)} dV}{\int |D^2(\vec{r}) e^{2\,i\,\vec{k}\cdot\vec{r}}|^2 dV}, \qquad (6)$$

where $\vec{r}$ is the vector position relative to the transducer, $D(\vec{r})$ is the beam directivity, $\vec{k}$ is the acoustic wavevector, $\vec{v}_t$ is the transverse velocity across the beam, τ is the time between pulse transmissions, and the integral is over the volume being sampled by the sonar. Standard deviations expected by combining (6) with (5) for beam 1 at a range of 60 cm are indicated by the solid line in Fig. 6. These theoretical values are about 20% less than the standard deviations determined using correlation coefficients, and about 40% less than the observed standard deviations.

From these comparisons it is clear that residual motions in the tow-tank do appear in the data but they do not dominate the velocity variance. The velocity standard deviations observed in the tow-tank are about 20% greater than would be expected based on the signal autocorrelation.

V. Velocity Accuracy

Velocity measurement accuracy is very high in monostatic Doppler sonars because velocity estimates are derived from phase shifts relative to a crystal oscillator. Difficulties do arise due to geometrical considerations and the bistatic system is much more sensitive in this regard than is a monostatic system. In Fig. 8 we provide an example of velocity calibration data for two orientations of the transducer array. Each data point in Fig. 8 represents the average of at least 250 independent velocity estimates made at a distance of 60 cm below the transducers. The data marked as for a 90° rotation corresponds to velocity in the Y-direction, data marked as for a 0° rotation has velocity in the X-direction (see Fig. 3b). The difference between the true and the observed speed (velocity magnitude) is plotted against the tow carriage speed. These results span the range of outcomes of our trials: some orientations give symmetrical results with respect to tow direction, others indicate an asymmetry in response as shown for the 0° data. Velocity bias indicated in Fig. 8 are typically less than 5% of the speed.

The data shown in Figs. 7 and 8 provide information on the measurement performance at a single depth but does not demonstrate the profiling capability of the system. In Fig. 9a and b, individual V and W component profiles are shown as solid lines for tow carriage speeds of 5.4, 20.6, 51.1, 101.9, 152.6, and 203.3 $\mathrm{cm\,s^{-1}}$. The transducer orientation for this

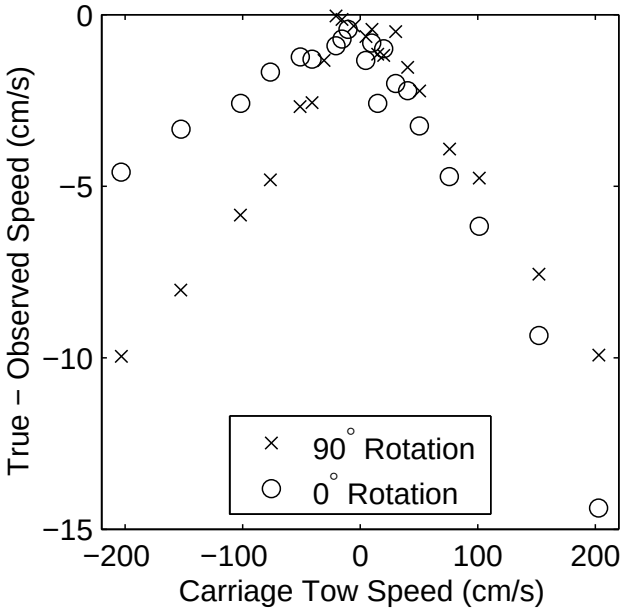

Figure 8: Velocity calibration data for two orientations of the transducer array. Each data point represents the average of at least 250 independent estimates at a range of 60 cm. The 90° orientation data (×'s) corresponds to a velocity in the Y-direction only, the 0° orientation data (○'s) has only an X component of velocity.

data was such that there is no U component of velocity (ie. the rotation angle $\alpha = 90°$). Dashed lines in Fig. 9a and b indicate the observed mean profiles. The vertical velocity profiles in Fig. 9b are offset by 10 cm s^{-1} to separate the successive plots. Notice that significant vertical structure is present in the vertical profiles at higher tow speeds. Similar vertical structure occurs in the horizontal velocities but it is small compared to the mean horizontal velocity. The large deviations seen in horizontal velocities beyond 70 cm range in Fig. 9a correspond to contamination caused by sidelobe interactions with the bottom (at 73.5 cm). The vertical orientation of the single (monostatic) system that derives vertical velocity is not subject to this interference and so no contamination is seen in Fig. 9b.

The present calibration results indicate a bias in velocity estimates of as much as 5% for some flow geometries. It is certainly conceivable that this bias might result from residual errors in the beam geometry estimate, but this cannot explain the asymmetry in bias that is seen in the 0° rotation data of Fig. 8 (and several other calibration runs). Velocity errors associated with errors in beam geometry will scale with tow speed and more importantly, they will always be symmetrical with respect to the tow direction. Errors associated with flow disturbance will also scale with tow speed, but they will only be symmetrical with respect to tow direction if the orientation

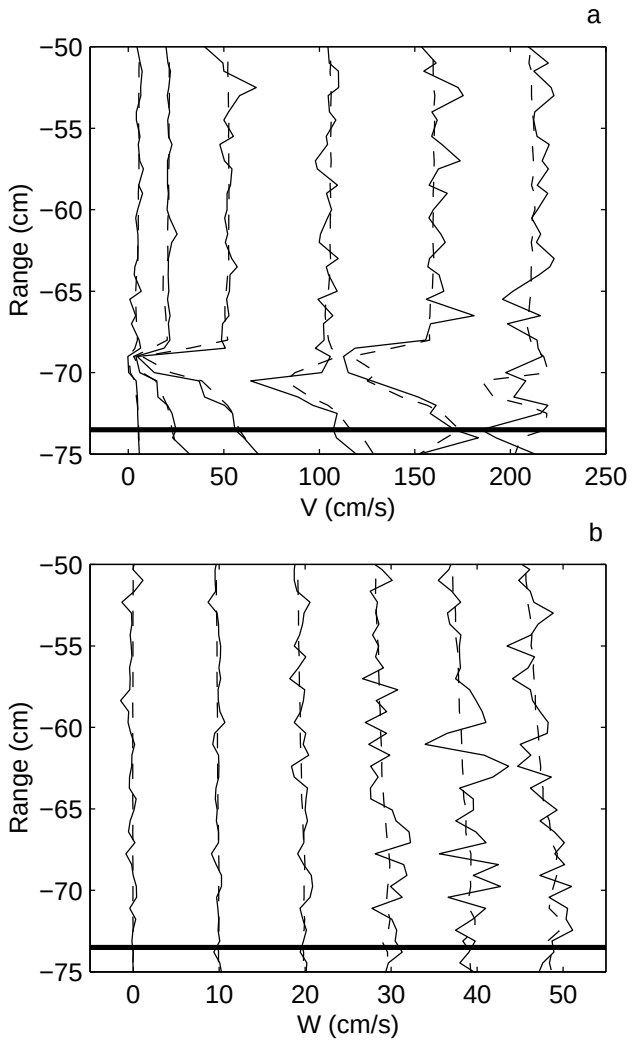

Figure 9: Profiles of a) horizontal (V), and b) vertical velocity for positive tow carriage speeds of 4.8, 20.0, 50.5, 101.3, 152.2, and 203.0 cm s^{-1}. Solid lines are individual profiles while dashed lines represent averaged profiles. Data are collected in the $\alpha = 90°$ rotation so that the U component of velocity is small. All vertical velocities are less than 5 cm s^{-1}: profiles for successively increasing tow speeds are offset by 10 cm s^{-1} in b). The bottom is at a range of 73.5 cm and is indicated by the broad solid line.

of the instrumentation is symmetrical. We can use this fact to separate bias caused by beam geometry from that caused by flow disturbance.

Profiles of speed error and vertical velocity normalized by carriage tow speed were plotted for a variety of calibration speeds (Fig. 10 shows the results for the 30° and 80° instrument rotations and for speeds ranging from 30 to 200 cm s^{-1}). The 30° and 80° rotations were chosen for this example because they contrast symmetrical flow over the instrument for positive and negative tow velocities (the 80° rotation) with asymmetrical flow (the 30° rotation), (see

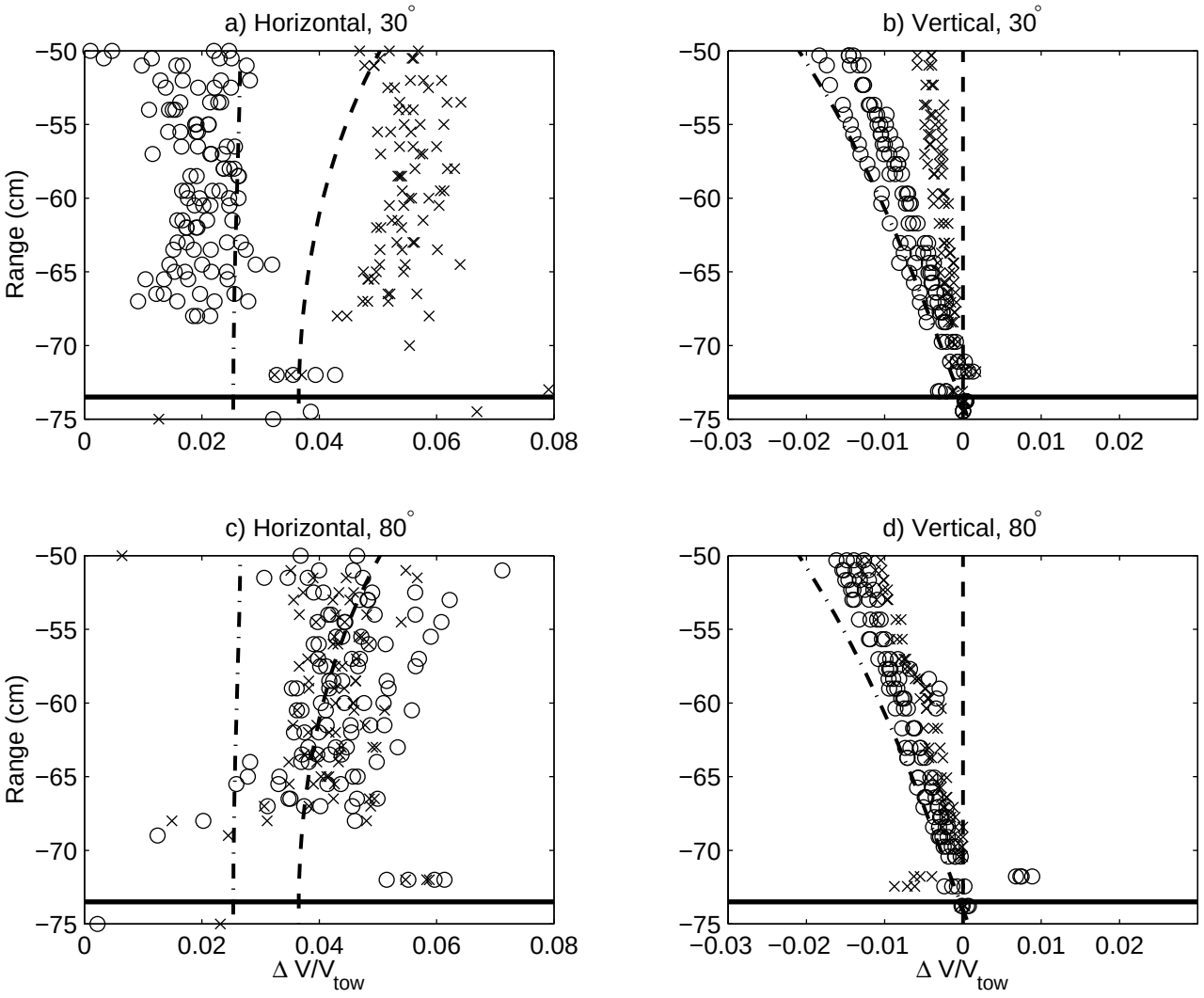

Figure 10: Tow speed normalized velocity errors for two tow orientations of the acoustic instrumentations; a) and b) are the horizontal (see (7)) and vertical speed errors for the 30° instrument orientation for tow speeds of -30, ± 50, ± 100, and ± 150 cm s^{-1}, c) and d) are the horizontal and vertical speed errors for the 80° instrument orientation for tow speeds of -40, ± 50, ± 75, ± 100, ± 150, ± 200 cm s^{-1}. In all cases, trials towed in a positive direction are indicated by ×'s, and trials towed in a negative direction are indicated by ∘'s. The bottom location is indicated by the solid line at a range of -73.5 cm. Velocity profiles predicted using potential flow around a 20 cm diameter cylinder are indicated by the dashed line (for velocities directly below the cylinder) and dash-dot line (for velocities 25 cm downstream of the cylinder).

Fig. 3a). The 90° and 0° rotations would have been the natural choice for this comparison, but a bottom bounce multiple in both of those trials introduces interference at the ranges between 65 and 70 cm. The operating configuration had been altered to eliminate this interference in the 30° and 80° rotation data sets. This interference is not obvious in Fig. 9a because the resulting deviations are small compared to the mean velocity.

In Fig. 10, speed error is determined as:

$$V_e = \frac{(\sqrt{U^2 + V^2 + W^2} - |V_c|)}{|V_c|}, \qquad (7)$$

where, V_c is the carriage tow speed, and (U, V, W) are the measured velocity components. Here, measured speeds greater than the carriage speed would be reported as a positive value irrespective of tow direction. In Figure 10, trials towed in a positive direction (corresponding to $U > 0$ in Fig. 3b) are indicated by ×'s, and trials towed in a negative direction are indicated by ∘'s. The bottom is located at a range of -73.5 cm indicated by a bold horizontal line in Fig. 10.

Vertical velocity data scaled as in Fig. 10b and d initially showed a great deal of scatter. This variability was caused by flexing of the instrument support

mast which changes the vertical orientation of the instrument. The resulting tilts cause a small component of the horizontal velocity to appear in the vertical velocity measurement. The magnitude of this effect can be determined by measuring the apparent vertical speed at the tank bottom. The mean tilt changes by as much as 0.5° between trials and varies by as much as 0.3° during a trial. The effects of this tilt have been removed from the data in Fig. 10 by subtracting the apparent speed of the bottom from the entire vertical velocity profile.

Comparing the horizontal speed results of Figures 10a, with 10c, the 30° rotation data has a marked asymmetry between positive and negative tow directions that is not seen in the 80° data. Differences are also seen in the vertical velocity data (Figures 10b, and d). The vertical velocity slope changes dramatically with tow direction in the 30° data where no such distinction occurs in the 80° data. Interpreting changes in observed bias between symmetrical and asymmetrical tow geometries as being associated with flow disturbance, the results suggest that most of the observed 5 % bias in horizontal velocities is caused by flow disturbance.

VI. Flow Disturbance

The instrumentation package was assembled to be as small as possible but it contains many bluff surfaces which will lead to flow separation and regions of turbulence. In this situation, it would be a major effort to model the flow around the instrument so as to provide an accurate verification of the observations. The magnitude of the instrument effect can however be arrived at by creating a two dimensional model based on the potential flow around a cylinder (see, for example, [8]).

As deployed, the instrument assembly has a thickness (vertical dimension) of about 15 cm and horizontal dimension of about 65 cm; it is held in position using a vertical mast made from 5 cm square stock attached at the center of the instrument array. Given the instrument dimensions, there is no obvious choice for a suitable cylinder diameter. Through the process of model testing, a 20 cm diameter cylinder was chosen because it gives vertical velocity anomalies that compare favorably with the observations. The cylinder was centered 74 cm above the bottom (an image surface): the presence of the water surface 1 m above the instrument was ignored. The predicted flow disturbance is indicated by contours of fractional horizontal velocity anomaly in Fig. 11a (using (7)), and by the vertical velocity anomaly (W/Carriage Speed) in Figure 11b. The data displayed in Figures 11a and b has been restricted to the range interval -75 to -50 cm corresponding to the sample interval of the observations and the horizontal range is constrained within 50 cm of the cylinder axis. In Figures 11a and b, the cylinder axis is located at the point $X = 0$, $Z = 0$.

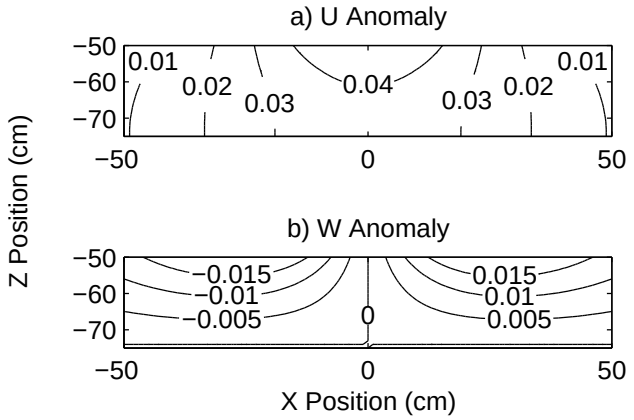

Figure 11: Contours of the a) horizontal and b) vertical velocity anomalies resulting from a 20 cm diameter cylinder positioned 74 cm above an image surface. The horizontal velocity anomaly is computed using (7), the vertical velocity anomaly is W/(tow speed). Only that vertical extent sampled by the Dopbeam system (-50 to -75 cm) is presented.

The model results show that the horizontal velocity anomaly (Fig. 11a) is maximum directly under the cylinder axis. It is fairly uniform over the depth interval sampled, and it does not change rapidly with horizontal position. The vertical velocity (Fig. 11b) is always zero at the bottom (Z = -74 cm) and increases in magnitude with height above the bottom. The vertical velocity is also zero in a line directly below the cylinder. In contrast to the horizontal velocity anomaly which is always positive (observed speed greater than the tow speed), the vertical velocity anomaly switches from negative values upstream of the cylinder (-X in Fig. 11b) to positive values on the downstream side.

In order to compare the model results directly with the observations, it is necessary to extract a single profile from the velocity sections shown in Fig. 11. The appropriate sample location is not obvious, and it changes as a function of tow direction and instrument rotation. Model profiles from X = -25 cm, corresponding to an upstream location and X = 0 cm directly below the instrument are plotted in Fig. 10 as dash-dot and dashed lines respectively The model was tuned to match the maximum observed vertical velocity error so that agreement in the maximum values of Fig. 10b and d is expected; the basic shape of the anomaly is however also consistent with the observations. The horizontal velocity anomalies (Fig. 10a and c) have values of 0.02 to 0.04 consistent in magnitude and depth structure with the observations.

Bias errors as large as 5% exist in the system even after accounting for beam geometry effects. The

model results suggest that errors of this order can be accounted for by flow disturbance from the instrumentation. For the 80° rotation data shown in Fig. 10c and d, the observed flow disturbance is in fact symmetrical with respect to tow direction consistent with the symmetrical geometry of the instrumentation (see Fig. 3b). In this geometry, the vertical velocity is measured directly under the center of the instrumentation so that, based on the model results, we would expect to observe zero vertical velocities. The occurrence of downward velocity at this rotation suggests that the effective center of flow disturbance is somewhat downstream of the instrument center as might be expected in the presence of flow separation off the abrupt edges presented at the back of the instrumentation. In contrast, zero vertical velocities are seen for the 30° rotation data in the positive tow direction. In this case, the vertical velocity is being measured at the trailing edge of the instrumentation (about 30 cm downstream of the instrument center) suggesting that this is close to the effective center of the disturbance.

VII. Conclusions

We have reported on the testing of a three element array 1.7 MHz coherent Doppler sonar systems in a bistatic configuration. By using modified beam patterns in a bistatic geometry we can extract profiles of three component velocities. These profiles are sampled simultaneously in time: samples in space are coincident within about ± 3 cm (as shown in Fig. 5). The vertical extent of the profiles depends on the instrument geometry; the data presented here allowed for profiles extending from 50 cm to 85 cm below the transducers in 0.7 cm range bins.

For the configuration example that we have presented, three component velocity profiles could be extracted over a depth interval from 50 cm to 85 cm. A greater depth interval could be achieved by aligning the transducers so that the intersection point occurred at a greater depth, or by reducing the separation between transducers. Such a change would however decrease the value of θ with a consequent degradation in the accuracy of horizontal velocity measurements as governed by (1) and (2).

An unavoidable difficulty with the bistatic geometry is that side-lobe contamination from the obliquely angled transducers interferes with horizontal velocity estimates close to the bottom. With the present system configuration, data within 4 cm of the bottom is contaminated by this effect (see Fig. 9a). Here again, adjustment of the operating configuration can be undertaken to minimize the degree of contamination. In particular, reducing the distance between the active and passive sonars would reduce the region of contamination but it would also degrade the accuracy of horizontal velocities.

The velocity measurements have been evaluated in two ways; random velocity fluctuations give rise to short term measurement uncertainties that could be reduced through averaging. The difference between long term velocity averages and the true (tow-carriage) speed is a measure of the absolute instrument accuracy or measurement bias.

Velocity calibrations show that bistatic component measurements have uncertainties similar to those occurring for monostatic systems. The accuracy results quoted here could therefore be adjusted for different system configurations subject to the constraints of monostatic coherent Doppler systems as described in [2]. Resolved horizontal velocity components sampled at 30 profiles/second have a short term uncertainty of about 5% of the measured velocity. (About 1% of this uncertainty is introduced by residual turbulence in the tow-tank.) Absolute accuracy for horizontal components is similarly on the order of 5%. In contrast, vertical velocity has a short term uncertainty of about 1% of the tow speed in the present tests and an overall accuracy of ± 0.5 $\mathrm{cm\,s^{-1}}$ can be achieved ([2]).

Two error sources that could contribute to the 5% bias in horizontal velocities are errors in system geometry, and flow disturbance around the instrumentation. The bistatic measurements are very sensitive to the exact geometry being used: geometry that is off by 1 cm can introduce a 1% bias in the resulting velocities. Great care was exercised in establishing exact (bistatic) beam patterns in order to determine the measurement geometry so that the existence of a 5% error was not expected. It is clear from the existence of structure in the vertical velocities (Fig. 8) that flow disturbance is caused by the instrumentation. In order to separate bias introduced from flow disturbance from that caused by errors in geometry, data was sorted according to tow direction and normalized by tow speed (see Fig. 10). Bias due to geometry errors will scale with speed and will change sign with changes in the sign of the true velocity: this error source should consequently always be symmetric with respect to tow direction. In contrast, errors caused by flow disturbance will scale with velocity but because of the complicated shape of the instrument array they will not in general be symmetric with respect to tow direction. Based on comparisons of velocity error for symmetric and asymmetric instrument orientations (Fig. 10), it is clear that the remaining 5% bias in horizontal velocity estimates is in part caused by flow disturbance.

All coherent sonar systems suffer from velocity ambiguity effects (see [5]). For the profiling bistatic system presented here, the maximum unambiguous velocity depends on scattering geometry and consequently it changes with depth. For the system as configured in these trials, the ambiguity speed for the bistatic beams varies from 11.6 $\mathrm{cm\,s^{-1}}$ to 11.1 $\mathrm{cm\,s^{-1}}$ (compared to 10.72 $\mathrm{cm\,s^{-1}}$ for the monostatic system). For currents that are dominated by horizontal components (as we expect in a near-shore environment), the maximum unambiguous horizontal velocity is about 40 $\mathrm{cm\,s^{-1}}$. For the tow-tank environment it is easy to accommodate the velocity wraps that occur because the true velocity is known in advance. The data presented have included observations of velocities adjusted over as many as three ambiguity speed crossings. For the case of field data, the raw component speed profiles must be evaluated to identify the large jumps in speed associated with crossings of the ambiguity velocity. The true velocity must then be reconstructed based on the time history or spatial evolution of the profiles. The sample pulse transmission rate can be altered to increase the ambiguity velocity ([2]), but because this parameter effects system accuracy such adjustments are not in general a solution to the problem. It is possible to use staggered pulse delays to extract the true velocity from the observations but we have not explored this technique. The occurrence of ambiguity speeds in coherent Doppler data remains an operational consideration.

The coherent Doppler profiling system has been developed for the purpose of observing sediment transport in the near-shore zone. In this environment, acoustic systems are attractive because they offer a non-intrusive means of observing velocities and suspended sediment concentrations. Despite the remote nature of the measurements, the present system introduces a flow disturbance of about 5% of the flow velocity. The platforms used to mount instrumentation in the near-shore environment are often much larger than the present instrument array as deployed in the tow-tank facility so that this sort of bias must exist in most field observations. The flow disturbance associated with a direct current measurement device would be potentially greater and this fact provides added incentive for the use of the acoustic systems in near-shore sediment transport studies.

Acknowledgement

The authors should like to acknowledge the support of Sontek in developing the Dopbeam coherent sonar system. Coordination of the many data streams could not have been achieved without software developed by Rob Craig controlling hardware designed and built by Wes Paul. In addition, this work could not have been undertaken without the use of the Memorial University Engineering tow-tank facility and the technical support of Andrew Kuczora. This research was funded by the Office of Naval Research Coastal Sciences Program, and the Natural Sciences and Engineering Research Council of Canada.

References

[1] A.E. Hay, and J. Sheng, "Vertical profiles of of suspended sand concentration and size from multifrequency acoustic backscatter," *J. Geophys. Res.*, pp. 15,661-15,677, 1992.

[2] L. Zedel, A.E. Hay, R. Cabrera, and A. Lohrmann, "Performance of a single-beam pulse-to-pulse coherent Doppler profiler," *J. Atmos. and Ocean. Tech.*, Vel. 21, No. 3, pp. 290-297, 1996.

[3] K.B. Theriault "Incoherent multibeam Doppler current profiler performance. Part I: Estimate variance," *IEEE J. Ocean Eng.*, OE-11, 7-15, 1986.

[4] B. Brumley, R. Cabrera, K. Deines, E. Terray, "Performance of a broad-band acoustic Doppler current profiler," *IEEE J. of Oceanic Eng.*, 16, 402-407, 1991.

[5] R. Lhermitte, and R. Serafin "Pulse-to-pulse coherent Doppler sonar signal processing techniques," *J. Atmos. and Ocean. Tech.*, Vol. 1, No. 4, pp. 293-308, 1984.

[6] R. Lhermitte, U. Lemmin, "Open-channel flow and turbulence measurement by high-resolution Doppler sonar," *J. Atmos. and Ocean. Tech.*, Vol. 11, No. 5, pp. 1295-1308, 1994.

[7] Kraus, N.C., A. Lohrmann, R. Cabrera: New acoustic meter for measuring 3D laboratory flows. J. Hydraulic Eng., 120, 406-412. 1994

[8] Kundu, P., "Fluid Mechanics", Academic Press, San Diego, p. 153, 1990.